Water Resources Research

RESEARCH ARTICLE
10.1029/2018WR022625

Key Points:
- From 1960–1987 and 1988–2015, 29% and 24% of the streamflow in the Copper River basin was simulated from glacier ice melt
- Trends of increasing temperature and snowfall drove simulated temporal differences in most, but not all, areas of the basin
- All subbasins lost simulated glacier storage over 1959–2015; only subbasins with small steep glaciers lost ice melt volume into streamflow

Supporting Information:
- Supporting Information S1

Correspondence to:
A. E. Van Beusekom,
beusekom@usgs.gov

Citation:
Van Beusekom, A. E., & Viger, R. J. (2018). A physically based daily simulation of the glacier-dominated hydrology of the Copper River basin, Alaska. *Water Resources Research*, *54*, 4983–5000. https://doi.org/10.1029/2018WR022625

Received 21 JAN 2018
Accepted 11 MAY 2018
Accepted article online 29 JUN 2018
Published online 26 JUL 2018

A Physically Based Daily Simulation of the Glacier-Dominated Hydrology of the Copper River Basin, Alaska

Ashley E. Van Beusekom[1] and Roland J. Viger[2]

[1]USDA Forest Service International Institute of Tropical Forestry, Río Piedras, Puerto Rico, [2]US Geological Survey, Boulder, Colorado, USA

Abstract The large, highly glacierized Copper River basin is an important water resource for the south-central region of Alaska. Thus, information is needed on the reaction of its hydrologic timing and streamflow volumes to historical changes in climate, in order to assess the possible impact of future changes. However, the basin is remote, and therefore, it has proved difficult to collect field data in a frequent temporal and spatial manner. An extension of the distributed-parameter, physical-process code Precipitation Runoff Modeling System, PRMSglacier, has been specifically developed to simulate daily hydrology without requiring extensive input data. In this study, PRMSglacier was used to characterize the hydrology of the Copper River basin from 1959 to 2015. The basin was split into subbasins for specific regional climatic calibrations and finer resolution characterization. The model was calibrated and performed well against data of glacier mass balance, glacier area change, snow cover, gaged streamflow, evapotranspiration, and solar radiation. Ice melt contributed 26% of the total basin streamflow, with differences temporally from climate oscillations. Furthermore, differences were seen geographically in subbasins depending on the state of the glaciers in each subbasin. Decreasing trends in ice melt volume were mostly seen on smaller steeper glaciers responding to a critical level of glacier recession, while increasing trends in ice melt volume were mostly seen on larger valley glaciers responding to increasing temperature. The areas with substantially decreasing ice melt had decreasing streamflow, possibly indicating health concerns for the ecosystems therein.

1. Introduction

The Copper River basin (61,952 km^2) is a large contributor to the Gulf of Alaska (GOA) and contains the one of the most important salmon habitats in Alaska for commercial and subsistence uses. Its resources are under increasing pressure with elevated use and development not only from fishing but also from mining, cabin building, recreational boating, off-road vehicles, and the Trans-Alaska Pipeline (Bidlack et al., 2014). The basin is also highly glacierized, and retreating glaciers are expected to affect the future timing and magnitude of its hydrology. However, this region is also one of the least measured areas in Alaska, and thus lacks detailed information on its hydrological timing, streamflow volumes, glacial component, and the historical changes therein, with which to assess the possible impact of future changes.

Recently, simulation codes have been developed for modeling the hydrological systems of large glacierized basins, explicitly accounting for hydrologic interactions between land and glacierized surfaces necessary to characterize these systems. However, these codes have relatively high input data requirements, such as detailed glacier basal topography (e.g., Clarke et al., 2015; Naz et al., 2014), and detailed subdaily weather data such as wind, radiation, and humidity (e.g., Beamer et al., 2016; Mernild et al., 2017), which are not available in most of the Copper River basin. Furthermore, these types of data that do exist are not reliable past the most historically recent decades. A recent study suggests that in data scarce areas, increasing model complexity will make the model more sensitive to input data errors and will not increase model performance (Tarasova et al., 2016).

Van Beusekom and Viger (2016) introduced and successfully demonstrated a glacier simulation code, PRMSglacier, with fewer data requirements (e.g., basal topography was inferred and weather data only required a daily time step), on two small basins in different hydro-climate zones in Alaska. That study documented the addition of a module to simulate glacier dynamics to an existing modular, deterministic, distributed-parameter, physical-process daily time step hydrological simulation code, Precipitation Runoff Modeling System (PRMS; Markstrom et al., 2015), for a new code PRMSglacier. The goal for building PRMSglacier was to contribute a broadly usable approach for integrating glacier dynamics into hydrologic simulation that balances the physical realism of a model with its usability in regional and remote watersheds. The design of PRMSglacier makes characterizing the hydrological system of the data-scarce Copper River basin possible. In this study, PRMSglacier is applied to the Copper River basin from 1959 to 2015, and the implications of its current hydrology and historical changes in hydrology are discussed. The hydrological changes include shifts in relative contributions from snow, ice, and rain, and also adjustments in longer-term storage components, in response to changes in historical climate conditions. This study does not model hydrology with projected future climate, but instead focuses on understanding potential vulnerabilities of the region to climate changes, after modeling the historical hydrological response. As a secondary result, this study extends methods from Van Beusekom and Viger (2016) by scaling to regional scale, which requires more sophisticated techniques for calibration across a large number of glaciers in different hydroclimatic and physiographic settings, while compensating for a drastically reduced availability of relevant data.

2. Study Area and Previous Work

The Copper River basin (Figure 1) is the sixth largest watershed by geographical area in Alaska and the second largest by streamflow runoff. The basin is rimmed above by mountains with peaks of 1,370–5,960 m (high point Mt Logan in Canada), including the Alaska Range in the north, the Wrangell-St. Elias Mountains in the east, and the Chugach Mountains in the south. The St. Elias Mountains contain nine of the 16 highest peaks in North America. In contrast, the lower river floodplain areas of the basin are ~50–1,200 m in elevation. These floodplain areas were created in major Pleistocene glaciations, during which the Copper River was dammed to make a proglacial lake covering most of the area west of the river between Chitina and Slana. Its retreat was responsible for the deposition of large amounts of clay sediment within the valley bottoms (Ferrians et al., 1989). Rivers mostly originate at glacier termini, and thus have characteristic braided floodplains working through glacial sediment and leaving level terraces on sides of the banks. Morainal hills exist away from the center of the basin, where the proglacial lake did not form (Ferrians et al., 1989).

The basin hosts two main climate zones, with glaciers in the temperature and precipitation extremes of these climate zones. The northern area is considered continental climate, with consistently low temperatures. The southern area is considered maritime, with large amounts of snowfall, but warmer temperatures (Bieniek et al., 2012). According to the Randolph Glacier Inventory 2009–2010 (RGI; Pfeffer et al., 2014), 20.1% of the basin was glacierized in 2010, with 178 glaciers that have an area larger than 5 km^2 (Figure 1). The interior of the basin between the Alaska Range and the Chugach Mountains experiences the continental climate with cold winters but, due to low elevation, has warm (and sunny) summers (Bieniek et al., 2012). There are only 3–5 hr of darkness in the middle of summer (3 in the north, 5 in the south) and conversely 3–5 hr of direct sunlight in the deepest of winter. Shallow permafrost covers the continental climate part of the basin with varying active-layer thickness (Pastick et al., 2015); spruce forests cover the wet areas with shallow permafrost. Shrubs grow in the floodplains and marshy areas, with more arid steppe-vegetation on south-facing drier slopes (Viereck et al., 1986).

For this study, the Copper River basin is defined as the area upslope of U.S. Geological Survey (USGS) gage 15214000 (Million Dollar Bridge, near Cordova). This location, 50 km upstream of the ocean, was chosen as the location of the downstream-most record of flow that lacked tidal or other ocean-related effects (such as glacier calving).

The Copper River basin hydrology has been previously modeled, mostly as part of larger studies looking at the contribution of freshwater to the GOA from the Copper and other basins. The studies made use of very different methods from this study to deal with the scarcity of data in the region. Older studies used relatively simplistic representations of glacier and hydrological dynamics (Royer, 1982; Wang et al., 2004), whereas newer studies used lumped estimates for glacier runoff based on regression-based estimates of hydrology (Hill et al., 2015; Neal et al., 2010). The newest study by Beamer et al. (2016) uses a deterministic, physical-process hydrological simulation code similar to this study; however, this GOA-wide application was only calibrated to four small watersheds with ideal data (on-glacier mass balance biannual measurements as well as higher quality stream gages than typical of the region), and so the authors cautioned against using the model to characterize hydrology in subsets of the GOA. Concurrently with the work presented in this paper, a conceptual monthly model of the Copper River basin hydrology was developed by Valentin et al. (2018) simulating historical streamflow (Valentin, Viger, et al., 2018) and projected streamflow (Valentin et al., 2018). The results of that coarser model will be compared to that of the model in section 5 of this paper.

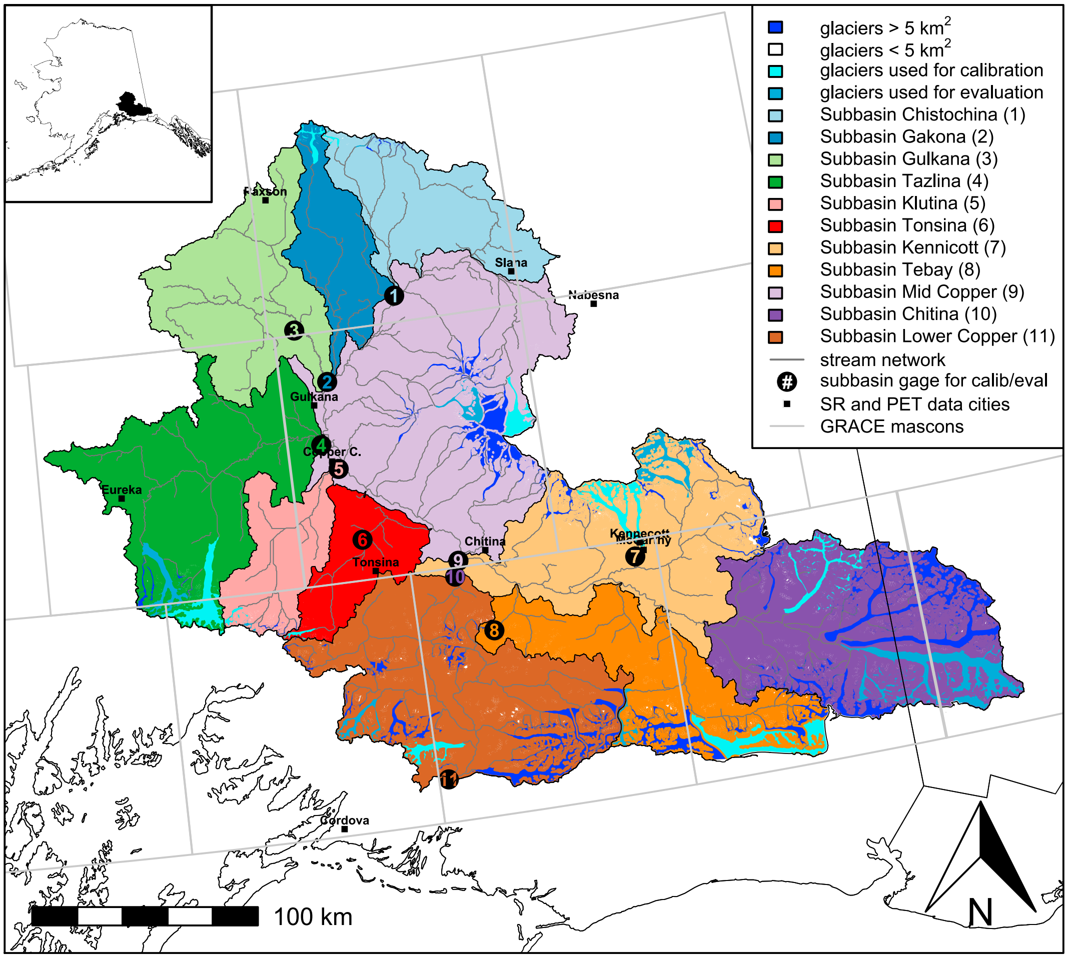

Figure 1. Copper River basin with locations of glaciers, subbasins, stream network (at selected coarseness for model), and gages, selected glaciers, and cities with solar radiation (SR) and potential evaporation (PET) data used for calibration and evaluation. All glacier extents are from the Randolph Glacier Inventory 2009–2010. Also pictured are the GRACE Space Flight Center (GSFC) solution mascons.

3. Methods

3.1. Glacierized Region Hydrological Simulation Code

PRMSglacier can be used to simulate land-surface hydrologic processes, including evapotranspiration, runoff, infiltration, shallow subsurface, groundwater, snowpack, soil moisture, glacier melt, and glacier area evolution, based on inputs of distributed daily maximum and minimum temperature and precipitation. The model calculates solar radiation (SR) and potential evapotranspiration (PET). The model was documented in Van Beusekom and Viger (2016); a brief overview follows, as well as a few small changes that were made to the code for use in this application. A figure of the model concept is included in Van Beusekom and Viger (2016).

3.1.1. Previously Documented PRMSglacier Code

Before beginning a PRMSglacier simulation, the basin needs to be partitioned into Hydrologic Response Units (HRUs) that are either standard or "glacier-capable." Each HRU is assumed to be homogenous with respect to its hydrologic response and should therefore be delineated to accommodate the dominant process in that location. Each HRU has parameters describing its topography, soils, vegetation type and density, and imperviousness, whether the HRU is glacier-capable, and, if so, the fraction to which it is glacierized at the beginning of the period of simulation. Each PRMSglacier HRUs is conceptualized as a series of reservoirs that include the soil zone, shallow subsurface, and groundwater reservoirs, whose outputs are combined to supply streamflow. Glacier-capable HRUs also have a glacier storage reservoir (although this can be empty if the degree of glacierization is zero). HRUs described as not being glacier-capable are referred to as "standard"

HRUs here. Normally, HRUs are exclusively delineated as left- and right-bank contributing areas to segments in the drainage network. In glacierized basins, an additional process is used to define HRUs within the area of each glacier as well as the maximum possible glacier extent within the period to be simulated. For each HRU, standard or glacierized, a water balance is computed each day and an energy balance is computed twice each day.

All fluxes from a given HRU are routed to a single segment in the drainage network, which directs flow through downstream network segments. These segments may flow across both nonglacierized and glacierized (i.e., beneath glaciers) land surfaces. The subglacial routing in the model does not represent dynamic interactions between subglacial streams and the overlying glacier, such as refreezing, hydraulic barriers, or englacial routing. However, this subglacial routing does allow the basal melt, controlled by a parameter indicating geothermal heating and friction, to be pushed to the HRU land surface below the glaciers (a small amount of water; Cuffey & Paterson, 2010), and it does allow direct tracking of flows that move beneath the glacier. Once in the network, water is routed to the basin outlet.

Melt of snow or ice on a glacierized HRU is determined by the model energy-balance calculations. For each glacier, there is a set of three reservoirs representing slow, medium, and fast rates of flow through the glacier (a theoretical construct of englacial flow from Baker et al., 1982). Every glacier-capable HRU is associated with a specific glacier. For a given time step, depending on the state of a given glacier-capable HRU, flows out of the HRU will be routed into one of these three (per-glacier) reservoirs. The outflow of these glacier-specific reservoirs is routed on a daily basis to the drainage network segment associated with the glacier terminus HRU. The terminus location changes with the evolution of the area of the glacier, which is determined by the model by applying the modified volume-area power law theory, relating the annual volume flux of the glacier, the basal slope of the glacier (estimated from surface simulation data), and the rate of mass turnover of the glacier (also from simulation data) to determine the new glacier area (Bahr et al., 1997; Lüthi, 2009). Full steady state adjustments likely take between decades and thousands of years, and estimates of these response times require very accurate glacier thickness calculations (Raper & Braithwaite, 2009). The area and equilibrium-line altitude for each glacier are calculated annually to generate smooth transitions between successive steady state areas (per Linsbauer et al., 2013) and help with calibration to infrequent measurements of glacier area. The model tracks when different sets of HRUs representing neighboring glaciers merge and break into discrete units. When these changes are detected, the model adjusts its per-glacier volume-area scaling and related calculations accordingly.

When a glacier-capable HRU transitions from completely to partially glacierized, the height of the newly exposed HRU surface is assumed to be the glacier basal elevation for that HRU (calculated with method of Mazo, 1995), and the fraction that remains glacierized (which generates ice melt) is reduced. The land in any HRU that is not beneath glaciers is modeled as intermittently impervious frozen ground based on an index that keeps track of daily HRU air temperature and continuous days below freezing for the HRU (Mastin, 2009; Mooers, 1990). Both standard and the portions of glacier-capable HRUs that are not glacierized can build a snowpack on the soil or rock surface of the land. HRU snowmelt infiltrates directly into the soil zone reservoir or runs off into the associated drainage network segment (as a result of soil saturation or infiltration excess).

3.1.2. PRMSglacier Version 2.0 Modifications

Numerous small glaciers exist in the Copper River basin as can be seen by the visual separation of glacier bigger and smaller than 5 km^2 in Figure 1. Delineating all these smaller glaciers into the number of elevation bands needed to drive the model calculations (at least three per glacier for basal topography calculations and at least two per glacier for variation in glacier-reservoirs) would have resulted in many miniscule HRUs whose size implied a precision that was inconsistent with the resolution of input and calibration data. Although it would have been convenient to simply eliminate these glaciers from the simulation, small glaciers can contribute substantially to runoff (Huss & Fischer, 2016). In order to accommodate representation of these smaller glaciers in a more practical manner, the PRMSglacier v.1 code (Van Beusekom & Viger, 2016) was augmented to characterize these glaciers as "glacierettes" and that contribute to the "glacierette fraction" of the each standard HRU. An HRU containing a nonzero glacierette fraction has a corresponding quantity of ice to melt once snowpack is depleted. HRU glacierette (ice) melt enters the stream network daily with no englacial lagging. Basal melt, calculated from the glacierette fraction of the HRU, infiltrates into the soil as with the glacierized HRUs. Change in the area of these glacierettes (ΔG) is calculated by the model every 10 years as a function of the initial glacierette fraction G_0, the temperature change from the initial conditions ΔT, and the initial elevation range of the ablation zone R_{abl} (estimated as the difference from the minimum elevation of the glacierette and the median elevation, $R_{abl} = Z_{median} - Z_{min}$). The area change function is

$$\Delta G = -G_0(170\ \Delta T)/R_{abl}, \tag{1}$$

This formulation assumes adjustment in the length of the ablation zone is geometric (Hagg et al., 2013) and a temperature-length adjustment rate of 170 m/°K (a conservative middle value of those measured, per Shea et al., 2015). Because there can be multiple glacierettes in a given HRU, the approximation is further simplified by using a mean of R_{abl} across all glacierettes in each HRU, and computing ΔG per HRU (per decade) with equation (1).

In order to simulate stream stage for calibration to gages without rating curves, the stream volume that is calculated by the model is transformed to depth using the classic power law hydraulic geometry assumptions, such that discharge Q is related to depth D as

$$D = c\ Q^b. \tag{2}$$

Parameters c and b need to be calibrated to the annual flow estimate; the exponent b is allowed between 0.1 and 0.7 with 0.2 a characteristic for braided glacial streams and 0.63 the value for a perfectly rectangular channel (Smith et al., 1996). Calibration uses measured streamflow as a target if possible, and measured stream stage only in areas with no streamflow available.

3.2. Data

3.2.1. Setup Data Sets

Digitized glacier outlines were taken from RGI 2009–2010 for glacier outlines, and a 100 m digital elevation model and stream network were derived from the 1 arc-second USGS National Elevation Database (https://viewer.nationalmap.gov/launch/, accessed January 2016). First, 1596 glacier-capable HRUs were delineated using 100 m elevation bands for HRU breakpoints on each glacier larger than 5 km^2, and drainage network segment was placed in each glacier-capable HRU. The level of 5 km^2 was arbitrarily set as the lower limit for "glacier" size, and the smaller ice bodies were modeled as glacierettes. Sensitivity tests found the volume of water coming from these glacierettes was miniscule compared to (large-sized) glacier runoff, so at the scale of the model, simulating the (more than 3,000) glacierettes as individual modeling response units would be a unwarranted addition of computational expense.

The glaciers were each given an extension in the nonglacierized land below their termini; the extensions were derived using the digital elevation model and the glacier shape (methodology: Van Beusekom & Viger, 2016). The extensions were then also subdivided into 100 m elevation bands. The remainder of the basin was then delineated into the left- and right-bank contributing areas associated with each link in the drainage network. The network was derived from a flow accumulation surface, as all cells whose values exceeded 100 km^2 drainage area. This topographic network was integrated with the glacier elevation-band segments and a subglacial connectivity network. The elevation bands for the glaciers and their extensions were merged, and the superimposed on the map of left- and right-bank contributing areas to produce the version of the HRU map used in the application. The Copper River basin delineations included a total of 2605 HRUs and 1989 stream segments. All HRUs were assigned parameters describing soil based on the USGS version of the USDA STATSGO2 database (NRCS; https://www.nrcs.usda.gov/wps/portal/nrcs/main/ak/soils/surveys, accessed January 2016) soil surveys, and vegetation based on the National Land Cover Database (NLCD 2011; https://www.mrlc.gov/nlcd11_data.php, accessed January 2016). Parameters that were not calculable in certain geographic areas (e.g., data were unavailable for Canadian lands or HRU was glacierized) were interpolated from surrounding area data and linear regression relationships from known locations.

Next, the basin was broken into 11 subbasins (Figure 1) to allow for finer-scale climate distribution and parameter calibration, ensuring that overall simulated water balance of the basin is good with specific geographical water fluxes characterized well. The geographical extent of each subbasin was chosen based on the location of a catchment for a stream gage, climate zone characteristics, and a necessary condition of subbasin-connectivity on the stream network. Subbasins included area outside of gage catchments (or excluded area inside) so that the basin was subdivided for rough climate zones (e.g., with delineation based on gage catchment alone, subbasin 7 would only include Kennicott Glacier and the rest of the area would be calibrated with subbasin 10; see Figure 1). Each subbasin was modeled starting in the 1950s because this was the earliest date for which maps showing glacier extent (USGS topographic map) for the entire basin were available. These maps were used to (manually) estimate the degree to which each glacier-capable HRU was glacierized. Several glaciers were joined in the 1950s that are not joined in 2009, so the model starts with 159 glaciers. The smaller glaciers, to be modeled as glacierettes, were expanded by increasing each HRU glacierette fraction greater than zero (from RGI) with equation (1) using the decadal average temperature change in the HRU from the Scenarios Network for Alaska and Arctic Planning (SNAP 2 km CRU TS; http://ckan.snap.uaf.edu/dataset/, accessed January 2016) temperature distribution in 2000–2010 to the SNAP distribution in 1949–1959. The subbasin models then start in the 1950s with 21.6% of the basin glacierized (as model units of glaciers or glacierettes), or 726 km^2 more glacierized area than in RGI 2009–2010.

3.2.2. Model Driver Data Sets

PRMSglacier needs daily maximum and minimum temperature and precipitation in each HRU to drive the models. Sparse and infrequently observed data are available, although most of these are from low elevation stations (away from glaciers). All publicly available data from various sources are collected in the Imiq database (http://arcticlcc.org/projects/imiq/, accessed January 2016). Details of the distribution of the Imiq database climate records daily to the HRUs are described in supporting Text S1 and Figure S1; here is a short summary.

Climate stations from the Imiq database within a 10 km buffer around each subbasin were used to derive daily station data for the HRUs within that subbasin. Climate station data were first corrected for systematic errors by using distribution mapping (Teutschbein & Seibert, 2012) to a high-spatial-resolution historical simulated climate product from the Weather Research and Forecasting model (hereafter referred to as the WRF model data; Monaghan et al., 2018). The WRF model data set, and other high-spatial-resolution climate data sets, is not available in the 1950 subbasin model start year. Thus, the available range of the WRF model data, water year (WY) 2003–2015, was used to establish a lapse rate from each climate station in the subbasin buffer to each associated subbasin HRU, per month. This relationship was then used to distribute daily data from available climate stations starting in the 1950s.

3.2.3. Data Sets Used in Calibration

Each of the 11 subbasins is calibrated in seven steps similar to Van Beusekom and Viger (2016), where the steps calibrate for seven hydrological system-influencing processes: (1) glacier mass balance and/or snow amounts, (2–4) flow volume and timing, (5) SR, (6) PET, and (7) glacier area change. The seven steps are run for five rounds. Each parameter is calibrated to minimize root-mean-square error objective function of simulation versus measurement in only one of the steps, according to which of the seven processes is most sensitive to the parameter (Van Beusekom & Viger, 2016; also see calibration parameters and ranges in the model archive associated with this manuscript; Van Beusekom & Viger, 2018). In this way, parameters mainly influencing glacier processes are calibrated separately from parameters mainly influencing nonglacier processes. This method reduces model equifinality but increases overall error relative to calibrating parameters to all objectives simultaneously (Chen et al., 2017). Within each calibration step, an objective function is identified and associated parameters are adjusted to minimize its value using the Shuffled Complex Evolution global search algorithm (Duan et al., 1994). The names of all calibration target data are listed in Figure 2, along with the period of record of the data. Of note, subbasin-wide snow volume adjustment to the distributed climate data (discussed in the last section) is calibrated in the first step. Subbasin-wide rain volume and temperature adjustments are calibrated in steps 2–4. Glacier capable HRUs in subbasins with over 20% glacierization (Kennicott, Tebay, Chitina, and Lower Copper) have separate temperature adjustment to compensate for possible errors in WRF representation of glacial microclimate (Cuffey & Paterson, 2010). All calibration targets are used with error bars, unless otherwise noted. In general, the calibration process attempted to minimize the objective function within the range of the error bars for the calibration data being used in a given calibration step. The first year of simulation was used as a model initialization period and was not used in calculating calibration objective functions.

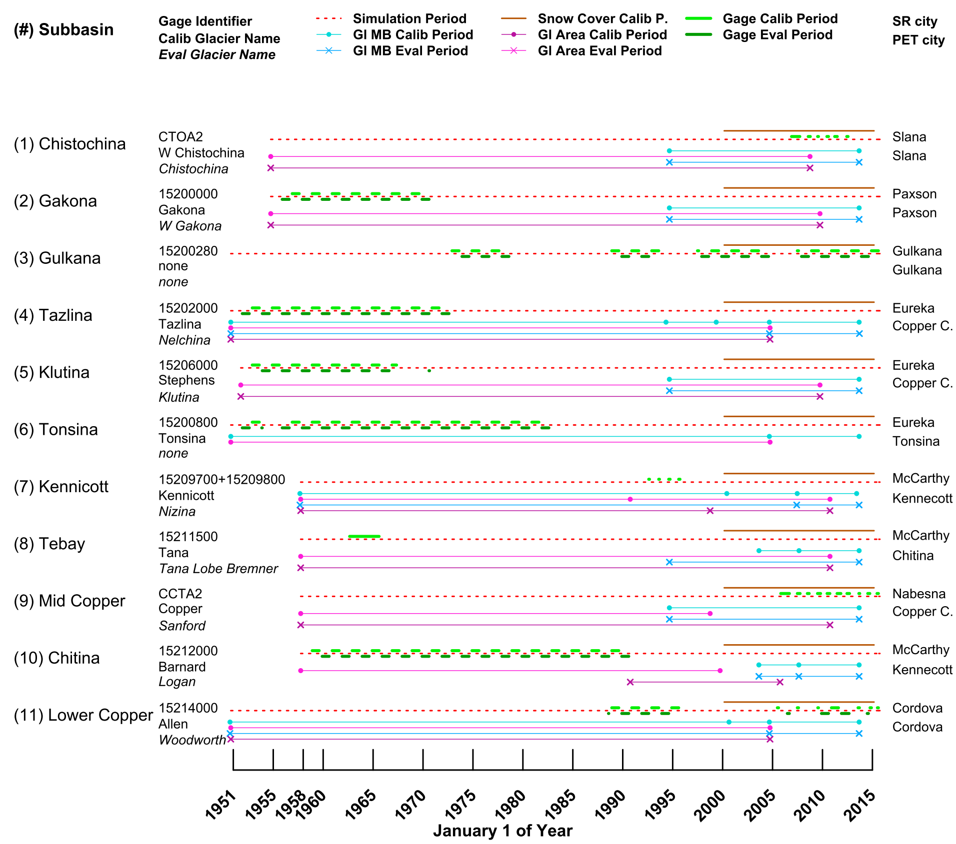

Figure 2. Period of record and location names for calibration and evaluation data sets. Gage data are daily measurements. Glacier mass balance (MB) and area values reflect change from the last measured value; actual measurement dates are indicated by dot or cross symbols, and a solid line for the period the change was measured over. Snow cover data are monthly averages. Mean monthly solar radiation (SR) and mean annual potential evapotranspiration (PET) data are calibrated to their targets for the entire period of model simulation.

All subbasins, except Gulkana, contain glaciers. In six of these, there was at least one glacier with data to inform calibration of parameters influencing both glacier mass balance and area change. The mass balance data are derived from repeat airborne altimetry and USGS topographic maps (Arendt et al., 2002, 2006, 2008, 2009; Das et al., 2014; Larsen et al., 2015), which are then used to calculate per-glacier changes in net mass balance over various time intervals with published error bars. In addition to using the same studies as for the mass balance data, glacier area information was supplemented with data from field studies (Wiles et al., 2002), RGI, Landsat images (Clarke & Holdsworth, 2002), and USGS topographic maps (USGS, 1968, 1969, 1970, 1973, 1977, 1978, 1980a, 1980b, 1983, 1986). There are no published error bars for the glacier area observations, so calibrations attempted to match these observations directly. For the four remaining subbasins, there were area change data but no information on glacier mass balances. For these subbasins, the glacier to the west of Chistochina glacier (referred to here as "W Chistochina"), Gakona, Stephens, and Copper Glaciers, the mean elevation change profile over the normalized glacier hypsometry curve of Larsen et al. (2015) with the published error bars was used as a proxy for the mass balance of these glaciers for calibration purposes. While the mass balance targets are single glaciers, the calibration target values influence the entire subbasin since glacier model parameters are calibrated subbasin-wide. Thus, the estimation of single-glacier mass balance target values by the regional-glacier mass balance Larsen values is considered valid. Names of calibration glacier by subbasin along with measurement days (and periods of time the cumulative measurements cover) are shown in Figure 2 (locations in Figure 1; each glacier is located within its subbasin). Because the mass balance data are only net change over a number of years and gives no information on interannual annual mass balance variability, monthly summaries of Moderate Resolution Imaging Spectroradiometer fractional snow cover area of each subbasin (MODIS SCA; Hall & Riggs, 2015) also were used to calibrate parameters influencing mass balance. Each MODIS cell has a daily snow cover binary report (snow covered or not) with an error of ±7% (Hall & Riggs, 2007). The cells are aggregated on a monthly basis and by subbasin; the errors are also aggregated for a calibration target error bar.

The USGS has 14 gages reporting daily flow volume in the basin within WYs 1951–2015; four of these gages (Bonanza Creek 15209750, Little Tonsina River 15207800, Sinona Creek 15199500, and Squirrel Creek 15208100) were not used in the study because their records were short in length and they were located in areas with other gages nearby. The Kennicott River has two forks; the larger West Fork gaged four years, while the gage on the smaller East Fork was only operating for one of those years. A total West and East Fork record of four years was synthesized by adding a percentage to the West Fork flow based on the year both forks had data. Because the flow for both forks is highly influenced by ice dam breakage around 4 July every year (Anderson et al., 2005), gage data from a week before through the week after the breakage were excluded from the model calibration. Gage locations for all of the gages used for calibration are identified by subbasin number in Figure 1. Periods of record and gage identifier numbers are given in Figure 2. Streamflow records from the USGS National Water Information System network were pulled by using the USGS Downsizer (Ward-Garrison et al., 2009) and separated into high and low flows with the Indicators of Hydrologic Alteration software (Richter et al., 1996). These gages are rated by the USGS as "poor" quality, meaning more than 15% error, so the error bars were set at ±20%.

Nine National Weather Service (NWS) gages were operated in the basin during this time (http://www.weather.gov/aprfc/rivobs, accessed January 2016), but only a few of these have rating-curves to calculate flow volumes from measured stream stage, and most are located very close to the USGS gage sites. The publisher characterizes all records as "preliminary" quality. Thus, data from these gages were only used at two of the locations, Chistochina River and Copper River above Chitina River. The steps for calibration using stage data (instead of flow observations) are annual calibration of flow magnitude, annual stage magnitude, and daily stage variability. These three steps correspond to steps 2, 3, and 4, respectively, in the calibration process used for the other nine basins. Magnitude of flow was approximated according to Jones and Glass (1993), which used basin area, average annual precipitation, and percentage glacier, to estimate basin-average annual flow volume. Jones and Glass (1993) reported that an error is ±12% with this method. Here the approximation parameters were fulfilled with the gage catchment area inside each subbasin, the average annual precipitation from SNAP data (1949–2010), and the estimated glacier cover in the starting model year. Error estimates on the stages were not available but were assumed to be high due to the difficult nature of collecting stream data in Alaska (personal communication with Edward Moran, NWS; 28 April 2016) and the error in the simplistic conversion of simulated flow to stage (equation (2)); therefore, the error bars were arbitrarily set at ±30%.

Subbasins 1 through 8 were calibrated to each of their gages. Subbasin 9 (Mid Copper) parameters were adjusted to best match the sum of within-subbasin flows and streamflow routed from subbasins 1 through 6. Subbasin 10 (Chitina) parameters were adjusted to best match the sum of within-subbasin flows and streamflow routed from subbasins 7, 8, and 9. Subbasin 11 (Lower Copper) parameters are then adjusted to best match the sum of within-subbasin flows and streamflow routed from subbasin 10.

Mean monthly SR calibration data sets were taken from the National Solar Radiation Database (http://rredc.nrel.gov/solar/old_data/nsrdb, accessed January 2016). The National Solar Radiation Database uses observed values when available, and modeled otherwise, at cities (necessarily lower elevation than the mountains). Mean monthly daily incoming shortwave SR values are given at a few cities for the periods of 1961–1990 and in more cities 1991–2010. Data for city stations that were not represented in the earlier period were extrapolated using the data from the stations that were in both periods. For PET, also collected at stations within cities, the calibration data set was the mean annual PET values taken from Patric and Black (1968). The model was calibrated to these mean monthly SR and mean annual PET values throughout the entire simulation. Neither SR nor PET was calibrated with error bars, as none are reported. See location of cities used in Figure 1 and cities by subbasin informed in Figure 2.

3.2.4. Evaluation Data Sets

Glacier mass balance and area were evaluated on one other glacier in each subbasin (see Figure 1 for locations and Figure 2 for periods), except Gulkana Subbasin, which has no glaciers, and Tonsina Subbasin, which has only one glacier over 5 km^2. The mass balance and area evaluation data were from the same studies as the calibration data; Chistochina, the glacier to the west of Gakona ("W Gakona"), Klutina, Tana lobe of Bremner, and Sanford Glaciers used the Larsen et al. (2015) calculations as a proxy for their mass balances. For 7 of the 11 stream gages, there was sufficient record length such that odd years were used for calibration and even years were left out for evaluation purposes (see gages in Figure 2).

Finally, total water storage simulated by the model in the entirety of the Copper River basin was compared to Gravity Recovery and Climate Experiment (GRACE) satellite data. GRACE uses coorbiting satellites to measure Earth and atmospheric mass changes. The terrestrial and cryosphere water storage change in these data (with removal of the glacial isostatic adjustment signal) is estimated at monthly time steps on equal-area, 1 arc-degree mass concentration cells, "mascons," by the Goddard Space Flight Center (GSFC) 2003–2016 (Luthcke et al., 2013). Each of the GSFC mascon solution water equivalent heights (GSFC.glb.200301_201607_v02.3b; http://ssed.gsfc.nasa.gov/grace/products.html, accessed August 2017) that intersected the basin was multiplied by its basin-intersection-area, and the volumes were summed for a total storage volume over the basin (see mascon boundaries in Figures 1; 11 mascons intersect the basin). The resolution of the mascon solution is quite coarse but allows for an independent source of data for evaluation.

4. Results

4.1. Calibration and Evaluation

All subbasin models begin with a year of initialization, after which model results are reported. The Nash-Sutcliffe efficiency metric (NSE; Nash & Sutcliffe, 1970) was used to assess model performance on daily streamflow, and daily stage in subbasins 1 and 9 where no streamflow data were available. The NSE is calculated as

$$\mathrm{NSE} = 1 - \sum \left(X^*_m(t) - X_s(t)\right)^2 / \sum \left(X^*_m(t) - \langle X^*_m \rangle\right)^2, \quad \text{for all times } t_0 \le t \le t_n, \tag{3}$$

where

$$X^*_m(t) = \begin{cases} X_s(t) & \text{if } X_m(t) - \varepsilon \le X_s(t) \le X_m(t) + \varepsilon \\ X_m(t) - \varepsilon & \text{if } X_s(t) < X_m(t) - \varepsilon \\ X_m(t) + \varepsilon & \text{if } X_s(t) > X_m(t) + \varepsilon \end{cases}, \tag{4}$$

and $X_m(t)$ is the measured value, ε is the error of the measurement, $X_s(t)$ is the simulated value, and $\langle X_m \rangle$ is the mean of the measured values over the calibration or evaluation period. An NSE of 1 is a perfect model, and a NSE > 0 says that the model is somewhat informative: that is, the model output is a more accurate than taking the mean of the measurements.

The absolute bias fraction (ABF) was used as a metric to assess model performance on glacier mass balance and area. Each glacier is a grouping of glacierized HRUs, and metrics are assessed over the whole glacier as it changes size. The ABF is calculated as the mean of all absolute values of bias fractions, with error, or:

$$\mathrm{ABF} = \sum \left| \left(X^*_m(t) - X_s(t)\right) / n X_m(t) \right|, \quad \text{for all times } t_0 \le t \le t_n, \tag{5}$$

with n representing the number of measurements and $X^*_m(t)$ representing the measured value, as in equation (3). Because error ranges were not available for glacier area, $\varepsilon = 0$ for area. An ABF of 0 is a perfect model.

Simulated and MODIS snow covered area was summarized by month and by subbasin, and compared using NSE. NSE was used as it is better suited than ABF for variables that frequently approach zero; whereas, ABF is a better metric for variables that do not have many measured values (e.g., mass balance).

Values for model performance metrics are given in Table 1; these are computed using error ranges of the measured values (if available). Note that SR and PET model simulation performance, and the annual average streamflow for subbasins 1 and 9, are not shown in Table 1 because simulated values fit the calibration targets almost perfectly and there were no evaluation data. Numbers of measurement points used in the metric calculations (n in equations (3) and (5)) are also given in the table.

4.2. Subbasin Differences

After initialization, the subbasin model simulations start in the range of WY 1952–1959, based on availability of input data (see Figure 2). The entire Copper River basin model is from WY 1959–2015, 56 years. The

Table 1
Model Performance for Calibration and Evaluation Periods for Copper River Subbasins

Subbasin	Metric quality	Daily stream NSE[a,b] Calibration	Daily stream NSE[a,b] Evaluation	Monthly Snowcover NSE[a]	Glacier MBChange ABF[c] Calibration	Glacier MBChange ABF[c] Evaluation	Glacier areaChange ABF[c] Calibration	Glacier areaChange ABF[c] Evaluation
(1) Chistochina	Metric Value[d]	1.00, 1.00[e]	NA	0.77	0.42	0.60	0.00	0.36
	Time Units Computed Over[f]	480 days	0 day	177 monthss	1 point	1 point	1 point	1 point
(2) Gakona	Metric Value[d]	0.74	0.44	0.84	0.01	0.40	0.00	0.10
	Time Units Computed Over[f]	2,555 days	2,924 days	177 months	1 point	1 point	1 point	1 point
(3) Gulkana	Metric Value[d]	0.01	−0.92	0.88	NA	NA	NA	NA
	Time Units Computed Over[f]	5,051 days	4,751 days	177 months	0 points	0 points	0 points	0 points
(4) Tazlina	Metric Value	0.75	0.79	0.93	0.26	0.58	0.00	1.79
	Time Units Computed Over[f]	3,650 days	4,021 days	177 months	4 points	2 points	1 point	1 point
(5) Klutina	Metric Value[d]	0.89	0.90	0.93	0.00	1.84	0.03	1.14
	Time Units Computed Over[f]	2,555 days	2,558 days	177 months	1 point	1 point	1 point	1 point
(6) Tonsina	Metric Value[d]	0.80	0.75	0.77	1.75	NA	0.00	NA
	Time Units Computed Over[f]	5,110 days	5,848 days	177 months	2 points	0 points	1 point	0 points
(7) Kennicott	Metric Value[d]	0.56	NA	0.78	6.90	0.56	0.04	0.94
	Time Units Computed Over[f]	511 days	0 days	177 months	3 points	2 points	2 points	2 points
(8) Tebay	Metric Value[d]	0.13	NA	0.72	4.64	0.0	0.01	0.99
	Time Units Computed Over[f]	823 days	0 days	177 months	2 points	1 point	1 point	1 point
(9) Mid Copper	Metric Value[d]	0.82, 0.87[e]	NA	0.95	0.00	0.32	0.01	6.79
	Time Units Computed Over[f]	2,002 days	0 days	177 months	1 point	1 point	1 point	1 point
(10) Chitina	Metric Value[d]	0.88	0.89	0.84	1.61	0.90	0.03	0.89
	Time Units Computed Over[f]	5,840 days	5,848 days	177 months	2 points	2 points	1 point	1 point
(11) Lower Copper	Metric Value[d]	0.77	0.83	0.77	1.40	2.36	0.01	2.20
	Time Units Computed Over[f]	2,444 days	2,294 days	177 months	3 points	2 points	1 point	1 point

[a]NSE (Nash-Sutcliffe efficiency) = 1.0 is perfect efficiency and decreasing values are decreasing efficiency. [b]The NSE for the stream metric is on streamflow volume in all subbasins except Chistochina and mid copper, which use stream stage height. [c]ABF (absolute bias fraction) = 0.0 is perfect and increasing values are decreasing goodness. [d]All metric computations take into account measurement error, except glacier area change which does not have error estimates. [e]First value is the NSE with daily streamflow (estimated with calibrated stage coefficient and exponent); the second value is the NSE with daily stream stage. [f]This is the number of time units the metric was computed over; in the case of glacier MB (mass balance) and area change the length of each unit differs.

simulated storage losses by subbasin (Figure 3a) were computed using the HRUs in each subbasin. Note that the subbasin total and glacier storage change (not actual storage) are initialized to 0 at the start of WY 1952 for ease of comparison. A negative storage change can be thought of as a storage loss since the beginning of the simulation. Glacier storage change includes only the storage change that happens on the glacierized areas (glaciers and the glacierettes), that is, what the models simulate on the glacierized areas for snowfall, internal accumulation with refreezing, snow and ice melt, glacier basal melt, and sublimation of snow and ice. Total storage change adds glacier storage change and also changes to all remaining (land-based) storage components, that is, what the models simulate for changes in storage in the nonglacierized snowpack, vegetation interception, soil moisture, impervious, shallow subsurface, and groundwater storage reservoirs. Because the Gulkana Subbasin has no glaciers, its glacier storage change is always zero. If the glacier storage changes in Figure 3 were subtracted from the total storage changes, the resulting plots would look similar to the Gulkana Subbasin plot with no glaciers; however, some basins show a systematic compounding difference in the storage changes that will be discussed in the next section. The GRACE solution has been found to be representative of the total storage change in the entire GOA basin (Beamer et al., 2016); here the total storage simulated in the Copper River basin (black line, Figures 3b and 3c) is compared to the GRACE GSFC solution over the Copper River basin (red line, Figures 3b and 3c).

The annual cycles of importance of ice melt to total streamflow are show in Figure 4. Day of year average flow simulated values over the subbasin simulation periods are shown in Figure 4(a). The black lines of total streamflow are not streamflow at the gages, but the streamflow contribution from the total area in each subbasin; the gage area is not equivalent to the subbasin area (see Figure 1). The simulated glacier ice contributions to subbasin streamflow are shown in purple; this glacier ice melt does not include melt from snow on the glaciers. The sum of the subbasin flow is the entire basin streamflow, shown in Figure 4b.

The mean ice melt and total streamflow for the first half of the simulation (28 WYs) and the second half are given in Table 2, by subbasin and total basin. These are the same as the numbers given in Figure 4, but

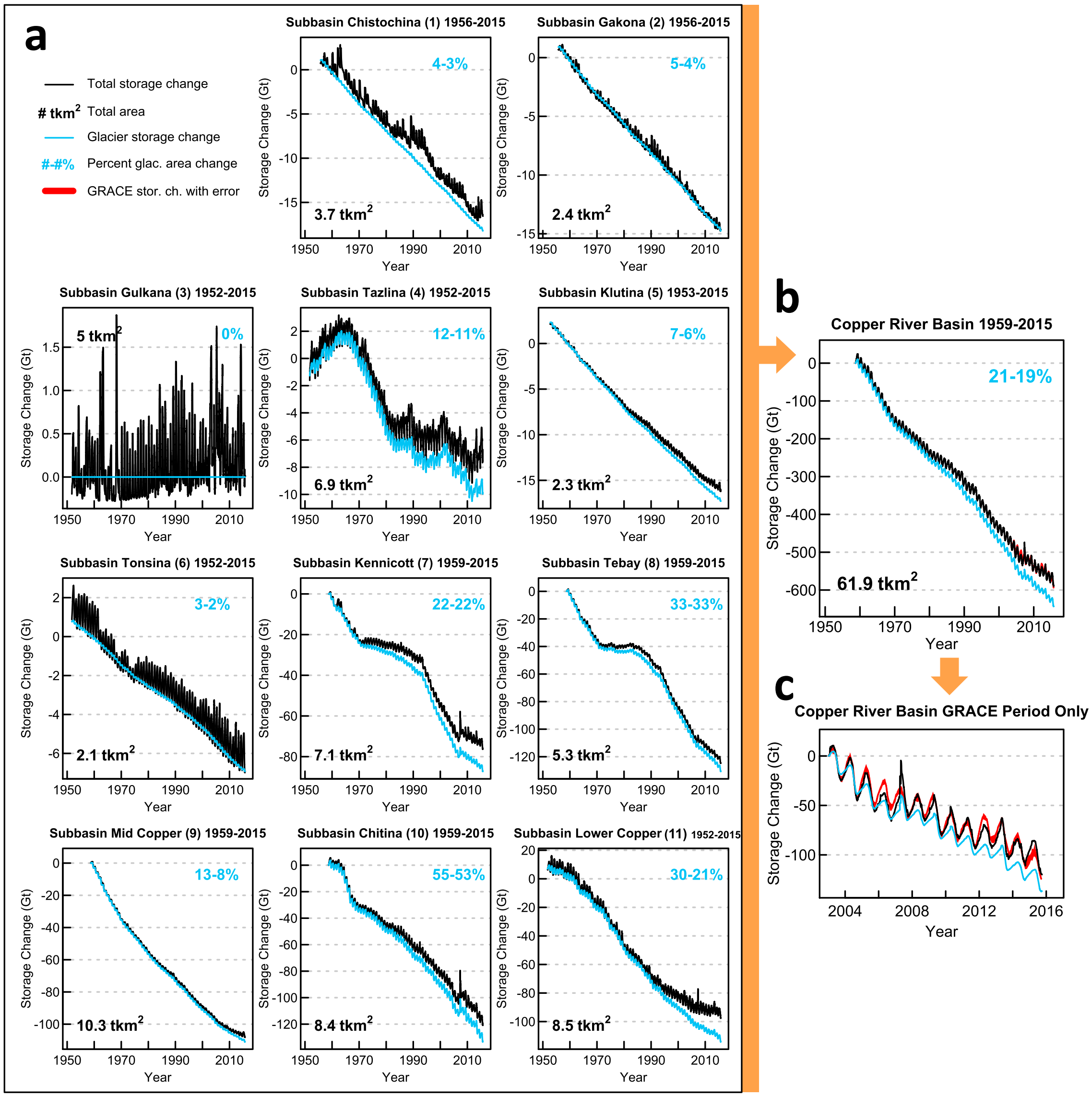

Figure 3. Simulated change in storage (units 1 Gt = 1 km^3): (a) in each subbasin and (b and c) the entire Copper River basin. Glacier storage change includes changes in ice and snow storage on the glaciers. All changes on plots (a) and (b) are zeroed at the start of WY 1959. Total subbasin (or basin) area is listed in the numbers inset on left of each subplot (units 1 "tkm^2" = 1,000 km^2) and percent glacierized area at the start and end of the simulation in the numbers inset on right of each subplot.

instead computed for two time periods instead of the whole period of simulation. The Mann Kendall (monotonic) trend test was performed on annual values of six variables for all HRUs, after testing for autocorrelation (Kendall, 1975; Mann, 1945). The results of the trend tests are plotted in Figure 5, with variables indirectly affecting (snow and ice) melt volumes in Figures 5a and 5c and variables directly contributing to streamflow volumes in Figures 5d and 5f.

5. Discussion

The model performance metrics show a good ability to simulate streamflow in a large, remote, glacierized basin, with evidence of model physical consistency from the ability to simulate glacier changes affecting streamflow. This claim is made on the basis that in both calibration and evaluation periods in most subbasins, streamflow NSEs are greater than 0.5, and cumulative glacier mass balance ABFs are less than 1.0. Furthermore, this physically based model, given the accurate simulations under changing historical climate conditions, could be expected to simulate hydrological responses under future climates, which were not

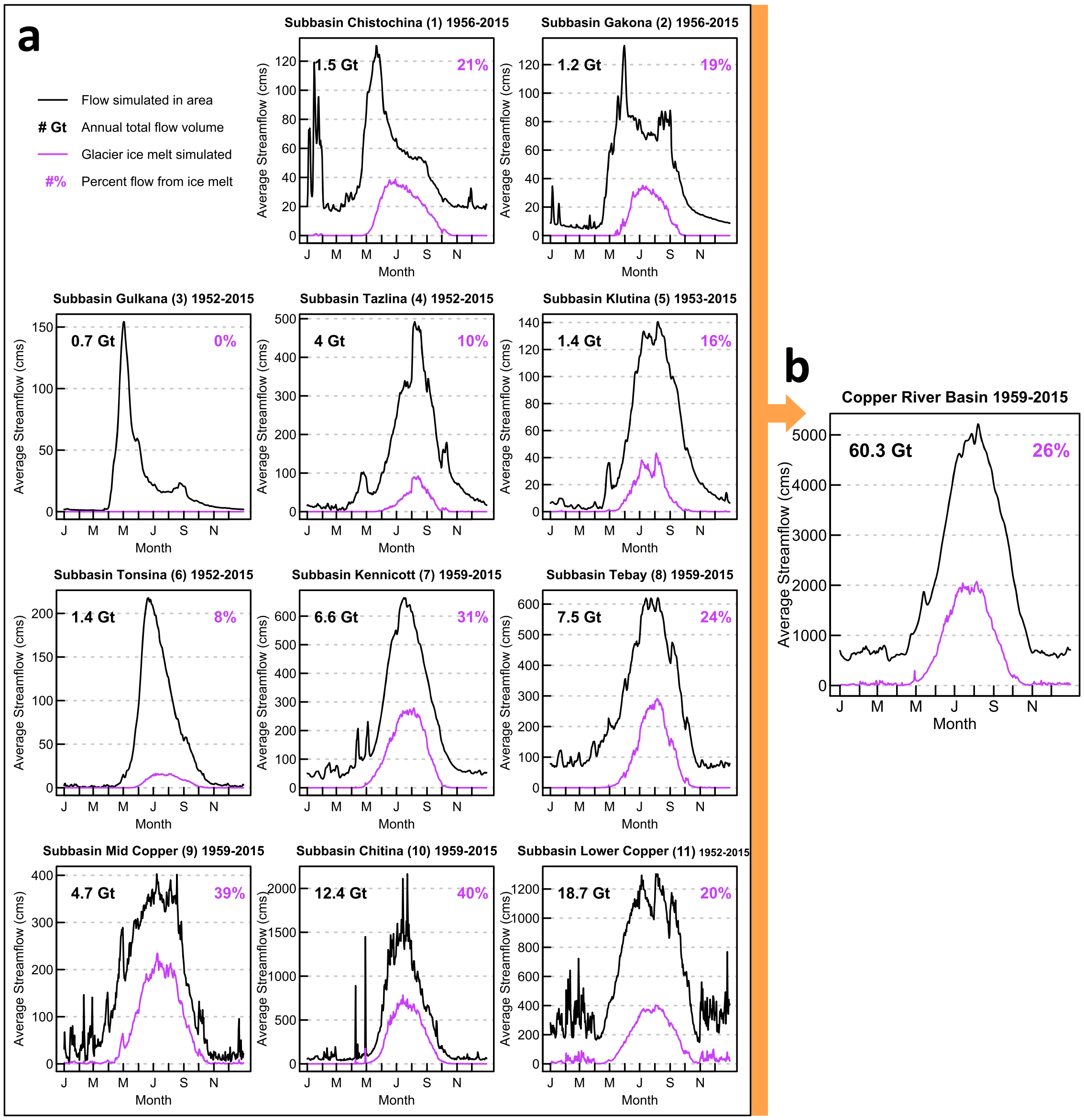

Figure 4. Simulated daily streamflow, and simulated daily glacier ice only melt, averaged over the period of simulation for each day of year, for the total area: (a) in each subbasin and (b) the entire Copper River basin. Average subbasin (or basin) annual flow is listed in the numbers inset on left of each subplot (units 1 Gt = 1 km^3) and average percent flow from ice melt in the numbers inset on right of each subplot.

present during the calibration period, a major advantage over statistical or more conceptual models. Calibration to observe snow-covered area data was relatively easy to fit (NSEs close to perfect efficiency). However, by integrating this spatially explicit information to the calibration process, multiyear cumulative mass balance targets of the reference glaciers could no longer be fit with a simple change in overall snow amounts. This additional constraint resulted in a more physically realistic model by reducing parameter equifinality (Frenierre & Mark, 2014). Although the calibration of glacier area change is also relatively trivial (ABFs effectively zero), this step is useful for constraining ice loss and testing the assumptions of the volume-area scaling in the subbasin, based on the results of the glacier area change ABF in the evaluation periods. These evaluation ABFs are generally close to 1.0. Departures from this general performance assessment will be discussed in the following sections on a subbasin-by-subbasin basis. These metric values are deemed good in regard to standards set by hydrologic modeling studies in a multitude of regions, and studies in glacierized regions (Moriasi et al., 2007; Tarasova et al., 2016).

Table 2
Average Annual Ice Melt Contribution to Total Flow, by Subbasin for First and Second Half of Simulation

	Mean annual ice melt (Gt)[a]		Mean annual flow (Gt)[a]		Percent ice melt of total flow	
Subbasin	1960–1987	1988–2015[b]	1960-1987	1988-2015[b]	1960-1987	1988-2015[b]
(1) Chistochina	0.35	0.35	1.62	1.81	21.6%	19.3%
(2) Gakona	0.26	0.26	0.98	1.83	26.3%	14.0%
(3) Gulkana	0	0	0.66	0.94	0%	0%
(4) Tazlina	0.54	0.46	4.18	5.00	12.8%	9.3%
(5) Klutina	0.27	0.24	1.52	1.67	17.7%	14.3%
(6) Tonsina	0.12	0.14	1.27	1.86	9.6%	7.6%
(7) Kennicott	1.96	2.71	6.38	8.98	30.7%	30.1%
(8) Tebay	1.67	2.56	7.71	10.28	23.2%	24.9%
(9) Mid Copper	2.61	1.67	5.91	4.98	44.1%	33.5%
(10) Chitina	5.26	6.09	11.30	17.47	46.6%	34.8%
(11) Lower Copper	4.72	4.02	20.50	23.41	23.0%	17.2%
Entire Copper	17.76	18.50	61.53	78.21	28.9%	23.7%

[a]1 Gt = 1 km^3. [b]The red indicates more than an 15% increase in the second period, the blue more than a 15% decrease.

Simulated water storage in the Copper River basin as a whole with seasonality removed shows a monotonic decreasing trend from the 1950s, with increasing or slower decreasing trends in many subbasins during the 1980s (Figure 3). This is consistent with glacier storage measured in the 1980s at two nearby glaciers, which saw increases at the maritime Wolverine Glacier (in the Kenai Mountains, southwest of the Copper River basin), and lessening-decreases at the continental Gulkana Glacier (in the Alaska Range, north of the basin) (Van Beusekom et al., 2010). The nonglacier storage can be seen to be increasing across the basin as whole and in many subbasins (see the systematic compounding of difference between blue and black lines in Figure 3). This is the result of increases in simulated nonglacier snowpack storage or groundwater storage. Off-glacier snowpack is most likely increasing because of climate driver data errors, as it is known glaciers that were not building in these areas. These errors have many potential sources, including but not limited to potential error in the WRF climate treatment of high elevation land with and without glacier cover, assumption of a stationary temporal pattern of the climate data for HRU distribution, and calibration adjustment of the resulting climate HRU distribution to targets of airborne altimetry (flight-path and not area-covering) mass balance data that may be biased too negative (Johnson et al., 2013).

Some nonglacierized HRUs do melt their annual snowpack but are still experiencing an increase in storage; precalibration simulations of groundwater flow to the stream were much higher than measured gage baseflow (interpreted as low flow during the winter season). Model parameters were then calibrated during winter to match the observed streamflow, which resulted in a reduced flux to streamflow, reserving flow into groundwater storage. This increasing storage agrees with GRACE observations in nonglacierized regions, which several authors have postulated is from permafrost degradation increasing groundwater storage (Muskett & Romanovsky, 2011; Riordan et al., 2006). The PRMSglacier model of the Copper River basin is not calibrated to the GRACE storage data; this data set is used for evaluation only. Agreement with GRACE and simulated land and ice storage change is good (Figure 3c).

The current study's finding of 26% of the flow from the Copper River basin coming from ice melt (Figure 4b) agrees with the earlier study of the basin by Neal et al. (2010), who estimated 14–33% of the flow came from ice melt by extrapolating the lidar mass balance data on from Arendt et al. (2002) on a several glaciers to the entire region. It also agrees with the monthly conceptual water balance model of the Copper River basin by Valentin et al. (Valentin, Viger, et al., 2018; value of 25% streamflow from ice melt). In the current study, the percentage of runoff coming from ice melt is larger per unit of glacier area in continental climates than in maritime climates. For example, the continental Chistochina and Gakona subbasins have ~4% glacier area (Figure 4a) with ~20% of streamflow from ice melt (Figure 3a), whereas the more maritime Tebay and Lower Copper subbasins have ~30% glacier area but only ~22% of streamflow from ice melt. This agrees with the study of O'Neel et al. (2014), which stated that loss or depletion of glacier mass will result in large

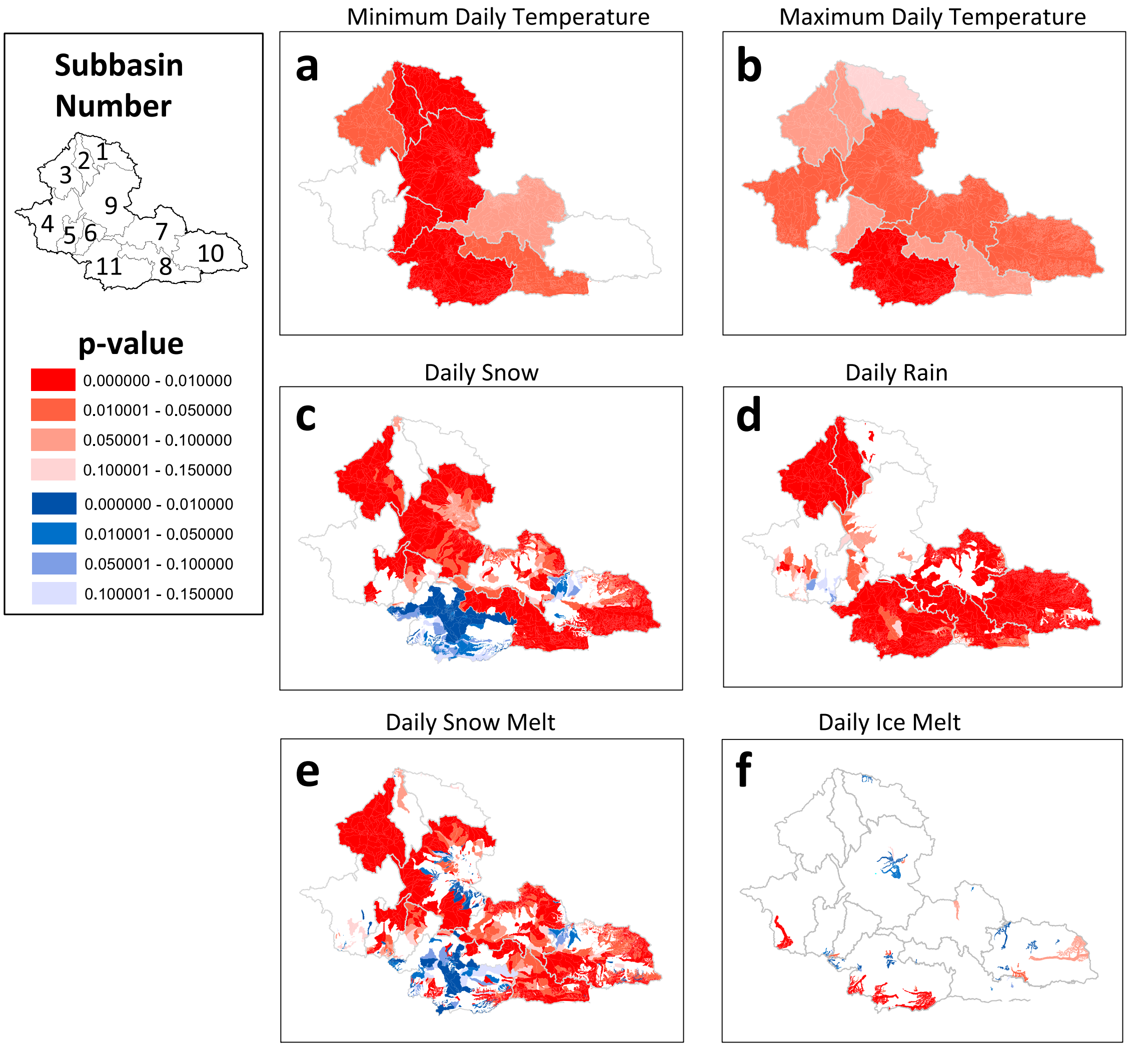

Figure 5. The *p*-values for Mann-Kendall trend tests with positive ? (the direction of the trend) in red and negative ? in blue. Subbasin boundaries are marked in gray. Tests were performed over the entire simulation period for annual HRU sums of daily: (a) minimum temperature, (b) maximum temperature, (c) snowfall, (d) rainfall, and (e) snowmelt, and for annual glacier or glacierette sums for (f) ice melt (colored at maximum extent from the beginning of the simulation). All plots have the same color-scale with the most significant trends in the darkest color, lessening in significance and lightening in color with white areas being non-detectable trend ($p > 0.15$). Note that $0.1 < p < 0.15$ is colored but is not typically considered a significant trend; the presence of color is used to show the areas that nearly have a significant trend and may influence differences seen in Table 2.

percentage changes in the volume of flow while the timing of peak flow periods are relatively stable in continental climate areas, whereas in maritime climate areas glacier melt will contribute less to streamflow and peak flow will move into a narrower time band earlier in the season (e.g., the pattern seen in the nonglacierized Gulkana subbasin in Figure 4a). The first and second periods separated in Table 2 contain more of the cool phase and more of the warm phases of the Pacific Decadal Oscillation (PDO), respectively. The warmer PDO phase has been shown to increase streamflow volumes in glacierized basins in Alaska with higher temperatures and snowfall, changes that are expected to amplify with future climate scenarios (Hodgkins, 2009). Table 2 shows that glacier ice melt contribution to flow did not decrease in volume substantially in the second period (again agreeing with Valentin, Viger, et al., 2018), except in subbasin 9 (Mid Copper). However, increases in streamflow from sources other than ice melt resulted in decreasing percentages of contribution of ice melt to total flow (Table 2), also capable of affecting peak flow timing.

The integrated simulation of the glacierized and nonglacierized hydrology of the Copper River basin, calibrated to subbasin-level with the physical processes modeled on a daily time step, makes it possible to characterize the hydrologic system of the basin in details that was not possible before this study. The increase in streamflow was caused by an increasing trend of more rainfall and snowmelt (from more snowfall and higher temperatures; Figure 5) over the period of simulation. This general basin pattern does not hold up in subbasin 11 and the east of subbasin 10 (Lower Copper and Chitina), here showing a decreasing trend in snowmelt along with a decreasing trend in snowfall. These areas are likely to have increased temperature so high that no precipitation falls as snow. Interestingly, the Mid Copper subbasin has a decreasing trend in high elevation snowmelt while showing an increasing trend in snowfall (Figure 5). It has the largest relative decrease of glacier area over the simulation period of any of the subbasins (Figure 3a), and the only substantial loss in ice melt and streamflow volume in the second half of the simulation (Table 2). The glaciers in this subbasin are steeper glaciers (mountain-top) than most of the valley glaciers in the basin and respond faster in recession to the warmer temperature regime of the later years of simulation (Lüthi, 2009). The glaciers appear to have been pushed past their critical point (Stahl et al., 2008): higher snow amounts do not add enough accumulation to offset glacier loss and higher temperatures no longer result in more ice melt to the system; here exhibiting the fragility of the mountain-top glacier regions during changes in climate. Basin-wide, the glaciers that had decreasing ice melt (Figure 5f) are overall much smaller than the glaciers with increasing ice melt, and the decreasing ice melt appears to be a reflection of decreasing glacier size (as opposed to increasing snow volumes absorbing part of the thermal budget prior to melting the glacier ice). Our interpretation that there will be a regime change for smaller glaciers is consistent with Valentin, Hogue, and Hay (2018). It appears that the trends found by the current study, when extended to 2100, would not confirm the conclusions of Valentin, Hogue, and Hay (2018) that glacier ice melt will increase in most areas and that streamflow will likely increase in all areas. This study agrees more with the wider GOA study by Beamer et al. (2017) showing reduction of glacier ice melt in the future. PRMSglacier could be used to forecast future streamflow in the Copper River basin with recently available daily time step climate forecasts (Walsh et al., 2018), but without these model runs, the ability to make more direct comparisons with studies of projected streamflow is limited. In general, care must be taken in synthesizing the results from different studies, especially if attempting to extrapolate from one period to another.

5.1. Known Subbasin Issues

The model is obviously responsive to the data used to set up, drive, and calibrate its application. Although the methods used to spatially distribute the climate data represent a balance between expense and quality of model performance, they are unfortunately far from ideal. Fitting monthly lapse rates to the WRF model data to distribute the climate station data acknowledges the large seasonal variation of spatial climate patterns in Southeastern Alaska (Monaghan et al., 2018) but does not account for interannual variability of these monthly lapse rates. The WRF model data lapse rates have a 2% variance on average, over the Copper River, for the 12 months and the 13 years of data. However, much higher variances (30–50%) are seen in the temperature lapses for the river valley HRUs in April and August, and hydrologically more importantly, in the precipitation lapses for the mountainside HRUs in February and August. Model quality could be improved if a high-quality daily climate reanalysis product was available, with a period of record long enough for calibration so that monthly lapse estimation would be not necessary. The daily climate product would need to date back to 1950, such that stream gage recording periods are covered. Without such a product, this study distributed climate in a coarse way, and used calibration targets to refine the climate, adjusting mean magnitude of temperature and precipitation inputs (see the model archive associated with this manuscript for calibrated parameters; Van Beusekom & Viger, 2018). It is a testament to the quality of the spatial distribution of the climate input that the calibrations are able to find trade-offs in fitting parameters for several kinds of calibration targets and that evaluation targets are also met. Glacier mass balances are most sensitive to precipitation overall volumes, whereas snow cover and streamflow are more sensitive to the distribution of climate input (Tarasova et al., 2016).

However, then with less-than-ideal climate input, inadequacies in calibration data become more of a problem than would be expected. Daily calibration targets are the most constraining; here the only daily data used is stream data. Subbasins with daily stream stage instead of stream volume are expected to have a lower performance (Chistochina and Mid Copper), as well as subbasins consistently missing data on a seasonal basin (only summer stream data at Chistochina, Kennicott, and Mid Copper). Spikes in simulated winter streamflow in these basins are evidenced to be a result of the lack of calibration constraint on daily winter runoff patterns

(Figure 4). While the spikes signify model issues, they represent a small temporal and volumetric aspect of the regional Copper River basin model (1) and do not negate the good model performance in the other aspects of these subbasins.

Model setup is most likely the cause of the issues in subbasins 3 and 8 (Gulkana and Tebay). The streamflow simulation in the Gulkana Subbasin is poor. With the proximity to the only nearly continuous daily climate station of Gulkana airport, as well as the lack of glaciers and thus high elevation area, this subbasin would be expected to be easy to model. However, the measured streamflow shows a large amount of baseflow and a late runoff peak that is characteristic of the hydrologic regime of a glacierized basin (Figure S2). It is possible that glacier flow is entering the subbasin outside of the topographically delineated model domain through groundwater sources (Valentin, Viger, et al., 2018); this interaction would be outside the scope of the model. Or, the gage has a large amount of error. Because the streamflow NSE metric (Table 1) is good for the Tonsina subbasin with only 3% glacierized area and 8% of flow coming from ice melt, it is not thought that this is an issue with how PRMSglacier is representing nonglacier cold-region processes. In the Tebay Subbasin, the gage catchment area is very small, 143 km^2. Possibly HRUs should be made smaller around this point if better performance is desired. In both these subbasins, good model metrics for the other calibration targets assure that the subbasin models are simulating the hydrology to the desired accuracy for the regional entire basin model.

PRMSglacier was designed to use few data inputs, and the Copper River basin model is one of the more extreme tests of its ability to do so. A need has been identified in the modeling community for more remotely sensed glacierized basin data (Moore et al., 2009); if more of such data becomes available, it could be straightforwardly incorporated into the Copper River basin model driver and calibration strategy.

6. Conclusions

PRMSglacier was successfully demonstrated on the Copper River basin, a large, remote basin without frequently collected temporal or spatial data. Calibration to multiple data sources separating out some glacier and snow processes reduced parameter equifinality and created a more physically consistent model. With this, the model is more conclusive in its characterization of the spatial response of the basin to the historical climate. Overall, warming temperatures corresponded with more streamflow but a decrease in the percentage contribution of glacier ice melt to that streamflow. However, in areas with smaller and steeper glaciers, the volumetric contribution of ice melt streamflow was also reduced with critical glacier loss. This shows that the glaciers in the basin can buffer the ecosystem from the effects of possible future climate warming to some extent, but the vulnerabilities will start showing with loss of mountaintop glaciers. Furthermore, reduction in percentage of flow coming from ice melt will alter peak flow timing even in areas that remain glacierized.

Acknowledgments
Output data are available at dx.doi.org/10.5066/P98HWKLJ. This work was supported by the Alaska Climate Adaptation Science Center and Northwest Climate Adaptation Science Center. Edward H. Moran and Andrew J. Monaghan provided data. Jessica M. Driscoll, Melissa McShea Valentin, Parker A. Norton, and Timothy P. Brabets provided data analysis. Lauren E. Hay provided comments on the manuscript, and we thank the anonymous reviewers whose comments improved the paper. Any use of trade, product, or firm names is for descriptive purposes only and does not imply endorsement by the U.S. government.

References

Anderson, R. S., Walder, J. S., Anderson, S. P., Trabant, D. C., & Fountain, A. G. (2005). The dynamic response of Kennicott Glacier, Alaska, USA, to the Hidden Creek Lake outburst flood. *Annals of Glaciology*, *40*, 237–242. https://doi.org/10.3189/172756405781813438

Arendt, A., Echelmeyer, K., Harrison, W., Lingle, C., Zirnheld, S., Valentine, V., et al. (2006). Updated estimates of glacier volume changes in the western Chugach Mountains, Alaska, and a comparison of regional extrapolation methods. *Journal of Geophysical Research*, *111*, F03019. https://doi.org/10.1029/2005JF000436

Arendt, A., Walsh, J., & Harrison, W. (2009). Changes of glaciers and climate in northwestern North America during the late twentieth century. *Journal of Climate*, *22*(15), 4117–4134. https://doi.org/10.1175/2009JCLI2784.1

Arendt, A. A., Echelmeyer, K. A., Harrison, W. D., Lingle, C. S., & Valentine, V. B. (2002). Rapid wastage of Alaska glaciers and their contribution to rising sea level. *Science*, *297*(5580), 382–386. https://doi.org/10.1126/science.1072497

Arendt, A. A., Luthcke, S. B., Larsen, C. F., Abdalati, W., Krabill, W. B., & Beedle, M. J. (2008). Validation of high-resolution GRACE mascon estimates of glacier mass changes in the St Elias Mountains, Alaska, USA, using aircraft laser altimetry. *Journal of Glaciology*, *54*(188), 778–787. https://doi.org/10.3189/002214308787780067

Bahr, D. B., Meier, M. F., & Peckham, S. D. (1997). The physical basis of glacier volume-area scaling. *Journal of Geophysical Research*, *102*(B9), 20,355–20,362. https://doi.org/10.1029/97JB01696

Baker, D., Escher-Vetter, H., Moser, H., Oerter, H., & Reinwarth, O. (1982). A glacier discharge model based on results from field studies of energy balance, water storage and flow. In J. W. Glen (Ed.), *Hydrological Aspects of Alpine and High-Mountain Areas, Proceedings of the Exeter Symposium 1982*, (pp. 101–112). Wallingford, UK: IAHS Publ.

Beamer, J., Hill, D., McGrath, D., Arendt, A., & Kienholz, C. (2017). Hydrologic impacts of changes in climate and glacier extent in the Gulf of Alaska watershed. *Water Resources Research*, *53*, 7502–7520. https://doi.org/10.1002/2016WR020033

Beamer, J. P., Hill, D. F., Arendt, A., & Liston, G. E. (2016). High-resolution modeling of coastal freshwater discharge and glacier mass balance in the Gulf of Alaska watershed. *Water Resources Research*, *52*, 3888–3909. https://doi.org/10.1002/2015WR018457

Bidlack, A. L., Benda, L. E., Miewald, T., Reeves, G. H., & McMahan, G. (2014). Identifying suitable habitat for Chinook salmon across a large, glaciated watershed. *Transactions of the American Fisheries Society*, *143*(3), 689–699. https://doi.org/10.1080/00028487.2014.880739
Bieniek, P. A., Bhatt, U. S., Thoman, R. L., Angeloff, H., Partain, J., Papineau, J., et al. (2012). Climate divisions for Alaska based on objective methods. *Journal of Applied Meteorology and Climatology*, *51*(7), 1276–1289. https://doi.org/10.1175/JAMC-D-11-0168.1
Chen, X., Long, D., Hong, Y., Zeng, C., & Yan, D. (2017). Improved modeling of snow and glacier melting by a progressive two-stage calibration strategy with GRACE and multisource data: How snow and glacier meltwater contributes to the runoff of the Upper Brahmaputra River basin? *Water Resources Research*, *53*, 2431–2466. https://doi.org/10.1002/2016WR019656
Clarke, G. K. C., & Holdsworth, G. (2002). Glaciers of the St. Elias mountains. US Geol. Surv. Prof. Pap.
Clarke, G. K. C., Jarosch, A. H., Anslow, F. S., Radić, V., & Menounos, B. (2015). Projected deglaciation of western Canada in the twenty-first century. *Nature Geoscience*, *8*(5), 372–377. https://doi.org/10.1038/ngeo2407
Cuffey, K. M., & Paterson, W. S. B. (2010). *The Physics of Glaciers*, (4th ed.). Oxford, UK: Academic Press.
Das, I., Hock, R., Berthier, E., & Lingle, C. S. (2014). 21st-century increase in glacier mass loss in the Wrangell Mountains, Alaska, USA, from airborne laser altimetry and satellite stereo imagery. *Journal of Glaciology*, *60*(220), 283–293. https://doi.org/10.3189/2014JoG13J119
Duan, Q., Sorooshian, S., & Gupta, V. K. (1994). Optimal use of the SCE-UA global optimization method for calibrating watershed models. *Journal of Hydrology*, *158*(3–4), 265–284. https://doi.org/10.1016/0022-1694(94)90057-4
Ferrians, O. J., Nichols, D. R., & Williams, J. R. (1989). Copper River basin. In T. L. Péwé, & R. D. Reger (Eds.), *Quaternary Geology and Permafrost Along the Richardson and Glen Highways Between Fairbanks and Anchorage*, (pp. 39–44). Alaska: American Geophysical Union. https://doi.org/10.1029/FT102p0039
Frenierre, J. L., & Mark, B. G. (2014). A review of methods for estimating the contribution of glacial meltwater to total watershed discharge. *Progress in Physical Geography*, *38*(2), 173–200. https://doi.org/10.1177/0309133313516161
Hagg, W., Hoelzle, M., Wagner, S., Mayr, E., & Klose, Z. (2013). Glacier and runoff changes in the Rukhk catchment, upper Amu-Darya basin until 2050. *Global Planet Change, Water in Central Asia – Perspectives under global change*, *110*(Part A), 62–73. https://doi.org/10.1016/j.gloplacha.2013.05.005
Hall, D. K., & Riggs, G. A. (2007). Accuracy assessment of the MODIS snow products. *Hydrological Processes*, *21*(12), 1534–1547. https://doi.org/10.1002/hyp.6715
Hall, D. K., & Riggs, G. A. (2015). *MODIS/Terra Snow Cover Monthly L3 Global 0.05Deg CMG*. Alaska Boulder Colorado: USA NASA Natl. Snow Ice Data Cent. Distrib. Act. Arch. Cent. https://doi.org/10.5067/MODIS/MOD10CM.006
Hill, D. F., Bruhis, N., Calos, S. E., Arendt, A., & Beamer, J. (2015). Spatial and temporal variability of freshwater discharge into the Gulf of Alaska. *Journal of Geophysical Research: Oceans*, *120*, 634–646. https://doi.org/10.1002/2014JC010395
Hodgkins, G. A. (2009). Streamflow changes in Alaska between the cool phase (1947–1976) and the warm phase (1977–2006) of the Pacific Decadal Oscillation: The influence of glaciers. *Water Resources Research*, *45*, W06502. https://doi.org/10.1029/2008WR007575
Huss, M., & Fischer, M. (2016). Sensitivity of very small glaciers in the Swiss Alps to future climate change. *Cryospheric Science*, *34*. https://doi.org/10.3389/feart.2016.00034
Johnson, A. J., Larsen, C. F., Murphy, N., Arendt, A. A., & Zirnheld, S. L. (2013). Mass balance in the Glacier Bay area of Alaska, USA, and British Columbia, Canada, 1995–2011, using airborne laser altimetry. *Journal of Glaciology*, *59*(216), 632–648. https://doi.org/10.3189/2013JoG12J101
Jones, S. H., & Glass, R. L. (1993). *Hydrologic and mass-movement hazards near McCarthy Wrangell-St Elias National Park and Preserve*, *USGS Numbered Series No. 93–4078*. Alaska: Water-Resources Investigations Report. U.S. Geological Survey.
Kendall, M. G. (1975). *Rank correlation methods*. London: Charles Griffin.
Larsen, C., Burgess, E., Arendt, A., O'Neel, S., Johnson, A., & Kienholz, C. (2015). Surface melt dominates Alaska glacier mass balance. *Geophysical Research Letters*, *42*, 5902–5908. https://doi.org/10.1002/2015GL064349
Linsbauer, A., Paul, F., Machguth, H., & Haeberli, W. (2013). Comparing three different methods to model scenarios of future glacier change in the Swiss Alps. *Annals of Glaciology*, *54*(63), 241–253. https://doi.org/10.3189/2013AoG63A400
Luthcke, S. B., Sabaka, T., Loomis, B., Arendt, A., McCarthy, J., & Camp, J. (2013). Antarctica, Greenland and Gulf of Alaska land-ice evolution from an iterated GRACE global mascon solution. *Journal of Glaciology*, *59*(216), 613–631. https://doi.org/10.3189/2013JoG12J147
Lüthi, M. P. (2009). Transient response of idealized glaciers to climate variations. *Journal of Glaciology*, *55*(193), 918–930. https://doi.org/10.3189/002214309790152519
Mann, H. B. (1945). Nonparametric tests against trend. *Econometrica*, *13*, 245–259. https://doi.org/10.2307/1907187
Markstrom, S. L., Regan, R. S., Hay, L. E., Viger, R. J., Webb, R. M., Payn, R. A., & LaFontaine, J. H. (2015). PRMS-IV, the precipitation-runoff modeling system, version 4. *US Geological Survey Technique and Methods*, 6–B7. https://doi.org/10.3133/tm6B7
Mastin, M. C., 2009. Watershed models for decision support for inflows to Potholes Reservoir. Wash. US Geol. Surv. Sci. Investig. Rep. 5081, 54.
Mazo, A. B. (1995). Selection of a quasisolution of the problem of recovering the balance curve of an alpine glacier. *Journal of Mathematical Sciences*, *74*(5), 1246–1250. https://doi.org/10.1007/BF02367690
Mernild, S. H., Liston, G. E., Hiemstra, C., Beckerman, A. P., Yde, J. C., & McPhee, J. (2017). The Andes Cordillera. Part IV: Spatio-temporal freshwater run-off distribution to adjacent seas (1979–2014). *International Journal of Climatology*, *37*(7), 3175–3196. https://doi.org/10.1002/joc.4922
Monaghan, A. J., Clark, M. P., Barlage, M. P., Newman, A. J., Xue, L., Arnold, J. R., & Rasmussen, R. M. (2018). High-resolution historical climate simulations over Alaska. *Journal of Applied Meteorology and Climatology*, *57*(3), 709–731. https://doi.org/10.1175/JAMC-D-17-0161.1
Mooers, H. D. (1990). A glacial-process model: The role of spatial and temporal variations in glacier thermal regime. *Geological Society of America Bulletin*, *102*, 243–251. https://doi.org/10.1130/0016-7606(1990)102<0243:AGPMTR>2.3.CO;2
Moore, R. D., Fleming, S. W., Menounos, B., Wheate, R., Fountain, A., Stahl, K., et al. (2009). Glacier change in western North America: Influences on hydrology, geomorphic hazards and water quality. *Hydrological Processes*, *23*(1), 42–61. https://doi.org/10.1002/hyp.7162
Moriasi, D. N., Arnold, J. G., Van Liew, M. W., Bingner, R. L., Harmel, R. D., & Veith, T. L. (2007). Model evaluation guidelines for systematic quantification of accuracy in watershed simulations. *Transactions of the ASABE*, *50*(3), 885–900. https://doi.org/10.13031/2013.23153
Muskett, R. R., & Romanovsky, V. E. (2011). Alaskan permafrost groundwater storage changes derived from GRACE and ground measurements. *Remote Sensing*, *3*(2), 378–397. https://doi.org/10.3390/rs3020378
Nash, J. E., & Sutcliffe, J. V. (1970). River flow forecasting through conceptual models part I—A discussion of principles. *Journal of Hydrology*, *10*(3), 282–290. https://doi.org/10.1016/0022-1694(70)90255-6
Naz, B. S., Frans, C. D., Clarke, G. K. C., Burns, P., & Lettenmaier, D. P. (2014). Modeling the effect of glacier recession on streamflow response using a coupled glacio-hydrological model. *Hydrology and Earth System Sciences*, *18*(2), 787–802. https://doi.org/10.5194/hess-18-787-2014

Neal, E. G., Hood, E., & Smikrud, K. (2010). Contribution of glacier runoff to freshwater discharge into the Gulf of Alaska. *Geophysical Research Letters*, *37*, L06404. https://doi.org/10.1029/2010GL042385

O'Neel, S., Hood, E., Arendt, A., & Sass, L. (2014). Assessing streamflow sensitivity to variations in glacier mass balance. *Climatic Change*, *123*(2), 329–341. https://doi.org/10.1007/s10584-013-1042-7

Pastick, N. J., Jorgenson, M. T., Wylie, B. K., Nield, S. J., Johnson, K. D., & Finley, A. O. (2015). Distribution of near-surface permafrost in Alaska: Estimates of present and future conditions. *Remote Sensing of Environment*, *168*, 15. https://doi.org/10.1016/j.rse.2015.07.019

Patric, J. H., & Black, P. E. (1968). *Potential evapotranspiration and climate in Alaska by Thornthwaite's classification. Pacific Northwest Forest and Range Experiment Station*. Juneau, Alaska: U.S. Dept. of Agriculture.

Pfeffer, W. T., Arendt, A. A., Bliss, A., Bolch, T., Cogley, J. G., Gardner, A. S., et al. (2014). The Randolph Glacier Inventory: A globally complete inventory of glaciers. *Journal of Glaciology*, *60*(221), 537–552. https://doi.org/10.3189/2014JoG13J176

Raper, S. C. B., & Braithwaite, R. J. (2009). Glacier volume response time and its links to climate and topography based on a conceptual model of glacier hypsometry. *The Cryosphere*, *3*(2), 183–194. https://doi.org/10.5194/tc-3-183-2009

Richter, B. D., Baumgartner, J. V., Powell, J., & Braun, D. P. (1996). A method for assessing hydrologic alteration within ecosystems. *Conservation Biology*, *10*(4), 1163–1174. https://doi.org/10.1046/j.1523-1739.1996.10041163.x

Riordan, B., Verbyla, D., & McGuire, A. D. (2006). Shrinking ponds in subarctic Alaska based on 1950–2002 remotely sensed images. *Journal of Geophysical Research*, *111*, G04002. https://doi.org/10.1029/2005JG000150

Royer, T. C. (1982). Coastal fresh water discharge in the northeast Pacific. *Journal of Geophysical Research*, *1978–2012*(87), 2017–2021. https://doi.org/10.1029/JC087iC03p02017

Shea, J. M., Immerzeel, W. W., Wagnon, P., Vincent, C., & Bajracharya, S. (2015). Modelling glacier change in the Everest region, Nepal Himalaya. *The Cryosphere*, *9*(3), 1105–1128. https://doi.org/10.5194/tc-9-1105-2015

Smith, L. C., Isacks, B. L., Bloom, A. L., & Murray, A. B. (1996). Estimation of discharge from three braided rivers using synthetic aperture radar satellite imagery: Potential application to ungaged basins. *Water Resources Research*, *32*(7), 2021–2034. https://doi.org/10.1029/96WR00752

Stahl, K., Moore, R. D., Shea, J. M., Hutchinson, D., & Cannon, A. J. (2008). Coupled modelling of glacier and streamflow response to future climate scenarios. *Water Resources Research*, *44*, W02422. https://doi.org/10.1029/2007WR005956

Tarasova, L., Knoche, M., Dietrich, J., & Merz, R. (2016). Effects of input discretization, model complexity, and calibration strategy on model performance in a data-scarce glacierized catchment in Central Asia. *Water Resources Research*, *52*, 4674–4699. https://doi.org/10.1002/2015WR018551

Teutschbein, C., & Seibert, J. (2012). Bias correction of regional climate model simulations for hydrological climate-change impact studies: Review and evaluation of different methods. *Journal of Hydrology*, *456*, 12–29.

U.S. Geological Survey (1968). *Tanacross 1956. Scale 1:250000*, *Alaska topographic series map N6300-W14700/60X180*, (). Reston, VA: U.S. Geological Survey.

U.S. Geological Survey (1969). *Gulkana 1959. Scale 1:250000*, *Alaska topographic series map N6200-W14400/60X180*, (). Reston, VA: U.S. Geological Survey.

U.S. Geological Survey (1970). *Mt. Hayes 1955. Scale 1:250000*, *Alaska topographic series map N6300-W14400/60X180*, (). Reston, VA: U.S. Geological Survey.

U.S. Geological Survey (1973). *Valdez 1960. Scale 1:250000*, *Alaska topographic series map N6100-W14400/60X180*, (). Reston, VA: U.S. Geological Survey.

U.S. Geological Survey (1977). *Cordova 1959. Scale 1:250000*, *Alaska topographic series map N6000-W14400/60X180*, (). Reston, VA: U.S. Geological Survey.

U.S. Geological Survey (1978). *Talkeetna Mountains 1954. Scale 1:250000*, *Alaska topographic series map N6200-W14100/60X180*, (). Reston, VA: U.S. Geological Survey.

U.S. Geological Survey (1980a). *McCarthy 1960. Scale 1:250000*, *Alaska topographic series map N6100-W14100/60X180*, (). Reston, VA: U.S. Geological Survey.

U.S. Geological Survey (1980b). *Nabesna 1960. Scale 1:250000*, *Alaska topographic series map N6200-W14100/60X180*, (). Reston, VA: U.S. Geological Survey.

U.S. Geological Survey (1983). *Bering glacier 1959. Scale 1:250000*, *Alaska topographic series map 60141-A1-TF-250*, (). Reston, VA: U.S. Geological Survey.

U.S. Geological Survey (1986). *Anchorage 1962. Scale 1:250000*, *Alaska topographic series map 61147-A1-TB-250*, (). Reston, VA: U.S. Geological Survey.

Valentin, M. M., Hogue, T. S., & Hay, L. E. (2018). Hydrologic regime changes in a high-latitude glacierized watershed under future climate conditions. *Water*, *10*(2), 128. https://doi.org/10.3390/w10020128

Valentin, M. M., Viger, R. J., Van Beusekom, A. E., Hay, L. E., Hogue, T. S., & Foks, N. L. (2018). Enhancement of a parsimonious water balance model to simulate surface hydrology in a glacierized watershed. *Journal of Geophysical Research: Earth Surface*, *123*, 1116–1132. https://doi.org/10.1029/2017JF004482

Van Beusekom, A., & Viger, R. (2016). A glacier runoff extension to the Precipitation Runoff Modeling System. *Journal of Geophysical Research: Earth Surface*, *121*, 2001–2021. https://doi.org/10.1002/2015JF003789

Van Beusekom, A. E., O'Neel, S. R., March, R. S., Sass, L. C., & Cox, L. H. (2010). Re-analysis of Alaskan benchmark glacier mass-balance data using the index method. US Geol. Surv. Sci. Investig. Rep. 5247, 16.

Van Beusekom, A. E., & Viger, R. J. (2018). *Supporting data for "A physically-based daily simulation of the glacier-dominated hydrology of the Copper River basin"*. Alaska: U.S. Geological Survey data release. https://doi.org/10.5066/P98HWKLJ

Viereck, L., Van Cleve, K., & Dyrness, C. (1986). Forest ecosystem distribution in the taiga environment, in: Forest ecosystems in the Alaskan Taiga. Springer, pp. 22–43.

Walsh, J. E., Bhatt, U. S., Littell, J. S., Leonawicz, M., Lindgren, M., Kurkowski, T. A., et al. (2018). Downscaling of climate model output for Alaskan stakeholders. *Environmental Modelling and Software*. https://doi.org/10.1016/j.envsoft.2018.03.021

Wang, J., Jin, M., Musgrave, D. L., & Ikeda, M. (2004). A hydrological digital elevation model for freshwater discharge into the Gulf of Alaska. *Journal of Geophysical Research*, *109*, C07009. https://doi.org/10.1029/2002JC001430

Ward-Garrison, C., Markstrom, S. L., & Hay, L. E. (2009). Downsizer—A graphical user interface-based application for browsing, acquiring, and formatting time-series data for hydrologic modeling. US Geol. Surv. Open-File Rep. 2009–1166 27.

Wiles, G. C., Jacoby, G. C., Davi, N. K., & McAllister, R. P. (2002). Late Holocene glacier fluctuations in the Wrangell Mountains, Alaska. *Geological Society of America Bulletin*, *114*, 896–908. https://doi.org/10.1130/0016-7606(2002)114<0896:LHGFIT>2.0.CO;2